PROTEIN STRUCTURE REPORT

Unfurling of the band 4.1, ezrin, radixin, moesin (FERM) domain of the merlin tumor suppressor

S. D. Yogesha,[1] Andrew J. Sharff,[2] Marco Giovannini,[3] Gerard Bricogne,[2] and Tina Izard[1]*

[1]Cell Adhesion Laboratory, Department of Cancer Biology, The Scripps Research Institute, Jupiter, Florida 33458
[2]Global Phasing Ltd., Sheraton House, Castle Park, Cambridge CB3 0AX, United Kingdom
[3]House Ear Institute, Center for Neural Tumor Research, Los Angeles, California 90057

Received 3 August 2011; Accepted 7 October 2011
DOI: 10.1002/pro.751
Published online 19 October 2011 proteinscience.org

Abstract: The merlin-1 tumor suppressor is encoded by the Neurofibromatosis-2 (Nf2) gene and loss-of-function Nf2 mutations lead to nervous system tumors in man and to several tumor types in mice. Merlin is an ERM (ezrin, radixin, moesin) family cytoskeletal protein that interacts with other ERM proteins and with components of cell–cell adherens junctions (AJs). Merlin stabilizes the links of AJs to the actin cytoskeleton. Thus, its loss destabilizes AJs, promoting cell migration and invasion, which in $Nf2^{+/-}$ mice leads to highly metastatic tumors. Paradoxically, the "closed" conformation of merlin-1, where its N-terminal four-point-one, ezrin, radixin, moesin (FERM) domain binds to its C-terminal tail domain, directs its tumor suppressor functions. Here we report the crystal structure of the human merlin-1 head domain when crystallized in the presence of its tail domain. Remarkably, unlike other ERM head–tail interactions, this structure suggests that binding of the tail provokes dimerization and dynamic movement and unfurling of the F2 motif of the FERM domain. We conclude the "closed" tumor suppressor conformer of merlin-1 is in fact an "open" dimer whose functions are disabled by Nf2 mutations that disrupt this architecture.

Keywords: actin cytoskeleton; adherens junctions; crystallography; neurofibromatosis

Introduction

Loss-of-function, generally nonsense point mutations in merlin manifest in familial *Nf2* lead to rare bilateral vestibular schwannoma and meningioma,[1] whereas biallelic inactivation of *Nf2* occurs in sporadic schwannoma,[2] meningiomas,[3] and malignant mesothelioma.[4] Furthermore, merlin proteins probably play broad roles in suppressing cancer, as heterozygous $Nf2^{+/-}$ mice, which express only half the level of these scaffold proteins in their tissues, are prone to developing a wide array of aggressive

Abbreviations: AJ, adherens junctions; CCP4, collaborative computational project Nr.4; ERM, ezrin, radixin, moesin; FERM, four-point-one ERM; *Nf2*, neurofibromatosis-2; NHERF, Na^+-H^+ exchanger regulatory factor; PEG, polyethylene glycol; PIP_2, phosphatidylinositol 4,5-bisphosphate.

Additional Supporting Information may be found in the online version of this article.

Grant sponsors: National Institutes of Health; State of Florida.

*Correspondence to: Tina Izard, Cell Adhesion Laboratory, Department of Cancer Biology, The Scripps Research Institute, Jupiter, FL 33458. E-mail: mkernick@scripps.edu

tumors, including sarcoma and carcinoma.[5,6] Merlin-1 and merlin-2 are unique amongst tumor suppressors in that they localize to and somehow stabilize maturing adherens junction (AJ) complexes that mediate cell–cell contacts[7] and that are directed by homotypic interactions of cadherin receptors. Further, merlin proteins also suppress the cell surface expression of transmembrane growth factor receptors.[8,9] Finally, they also associate with the actin network, either directly via interactions of their *N*-termini with actin,[10–12] or indirectly via heterotypic interactions with other ezrin, radixin, moesin (ERM) family members.[13] Importantly, these functions are necessary for proper development, cell growth, and contact inhibition, and for harnessing tumorigenesis.

ERM proteins provide essential links of AJs to the actin cytoskeleton,[14] play important roles in remodeling AJs during epithelial morphogenesis, and maintain organized apical surfaces on the plasma membrane.[10] ERM proteins belong to the band 4.1 superfamily that shares an ~300-residue globular FERM domain comprised of three subdomains (F1, F2, and F3), whose structure resembles that of a cloverleaf.[15] These proteins also harbor a central α-helical rod domain and a *C*-terminal domain that directs F-actin interactions. The overall architecture of merlin is thought to be similar to that of ERM proteins, as they have a FERM domain and a central α-helical rod, but lack a *C*-terminal actin-binding site.

All ERM proteins appear to be regulated by transitioning from a closed conformation to an open, active state following severing of intramolecular head–tail interactions, and of interactions between their head and central α-helical domains. The crystal structures of the FERM domains of ezrin and merlin,[16–18] the moesin head:tail complex, and the moesin FERM domain in complex with its central α-helical domain have been solved.[15,19] The moesin head:tail complex structure established that this interaction buries the charged F-actin binding site, and that the *C*-terminal tail covers large portions of the F2 and F3 motifs of the FERM domain. Conformational changes that occur when these proteins switch to their activated state are thought to sever these intramolecular contacts, allowing these proteins to open and bind to their other partners.

How ERM proteins are activated is not entirely resolved, but this is a Rho dependent process[20] and is triggered by binding to other protein ligands or phospholipids or by phosphorylation as seen with merlin-1.[21] For example, the binding of the FERM domain of ERM proteins to the cytoplasmic tails of ICAMs or the adaptor protein EBP50 displaces the ERM *C*-terminal tail despite their binding sites not overlapping.[22,23] Further, the binding of a basic cleft that lies between the F1 and F3 subdomains to phosphatidylinositol 4,5-bisphosphate (PIP_2) directs ERM proteins to the plasma membrane, and may also sever their head–tail interactions.[24] Finally, phosphorylation of conserved threonine residues in the ERM *C*-terminal actin-binding site is necessary for their localization to AJs and for binding to the actin cytoskeleton, and maintains ERM proteins in their active state. Probably all three triggers, phosphorylation and binding to PIP_2 and protein partners, is necessary for full activation of ERM proteins.[25]

What triggers sever the supposedly "closed," tumor suppressor-active form of merlin-1 is less clear, although Ser-10 and Ser-518 phosphorylation by PKA and/or PAK have been proposed to have a role in this response.[26,27] Further, phosphomimetic mutants of these sites impair merlin-1 tumor suppression functions and these mutants directly interact with other partners in cells, such as ezrin.[28] Binding partners for ERM proteins include each other, and selected adhesion proteins and adapters that direct association with membrane-spanning proteins. For example, the *C*-terminal domains of the EBP50 and E3KARP members of the NHERF (Na^+-H^+ Exchanger Regulatory Factor) family bind to ezrin and merlin, and link ERMs to membrane proteins such as NHE3 and CTFR through the agency of their PDZ domains.[29] In addition, ERM proteins and merlin also directly bind to adhesion receptors, including NHERF,[30] CD44,[31] and E-cadherin.[7]

To define the ostensibly closed, tumor suppressor-active state of merlin-1, we crystallized the human merlin-1 head:tail complex. While no electron density is visible for the tail domain in this structure the F2 domain is unfurled, suggesting that binding of the merlin-1 tail promotes movement and unfurling of its F2 motif. Thus, merlin is actually in an "open" conformation relative to other ERM members, perhaps explaining its tumor suppressor function.

Results

Overall crystal structure

We copurified the merlin-1 head and tail domains and crystallized the head:tail complex. SDS-PAGE (SDY, unpublished data) and mass spectrometry analyses confirmed the presence of the tail domain in these crystals (Supporting Information Table). However, electron density was only observed for the head domain. The final model is comprised of residues 20–82, 91–152, 178–312 (chain "A"); 20–82, 91–152, 178–312 ("B"); 20–82, 91–158, 178–312 ("C"); and 20–82, 91–150, and 199–312 ("D"). As seen in other isolated FERM domain structures, and in the moesin head:tail structure,[15] the structure of the merlin head domains harbors three subdomains (F1, F2, and F3) [Fig. 1(A)] having fold similarities to known single-domain proteins.[32] The F1 subdomain resembles ubiquitin, whereas F2 shares structural

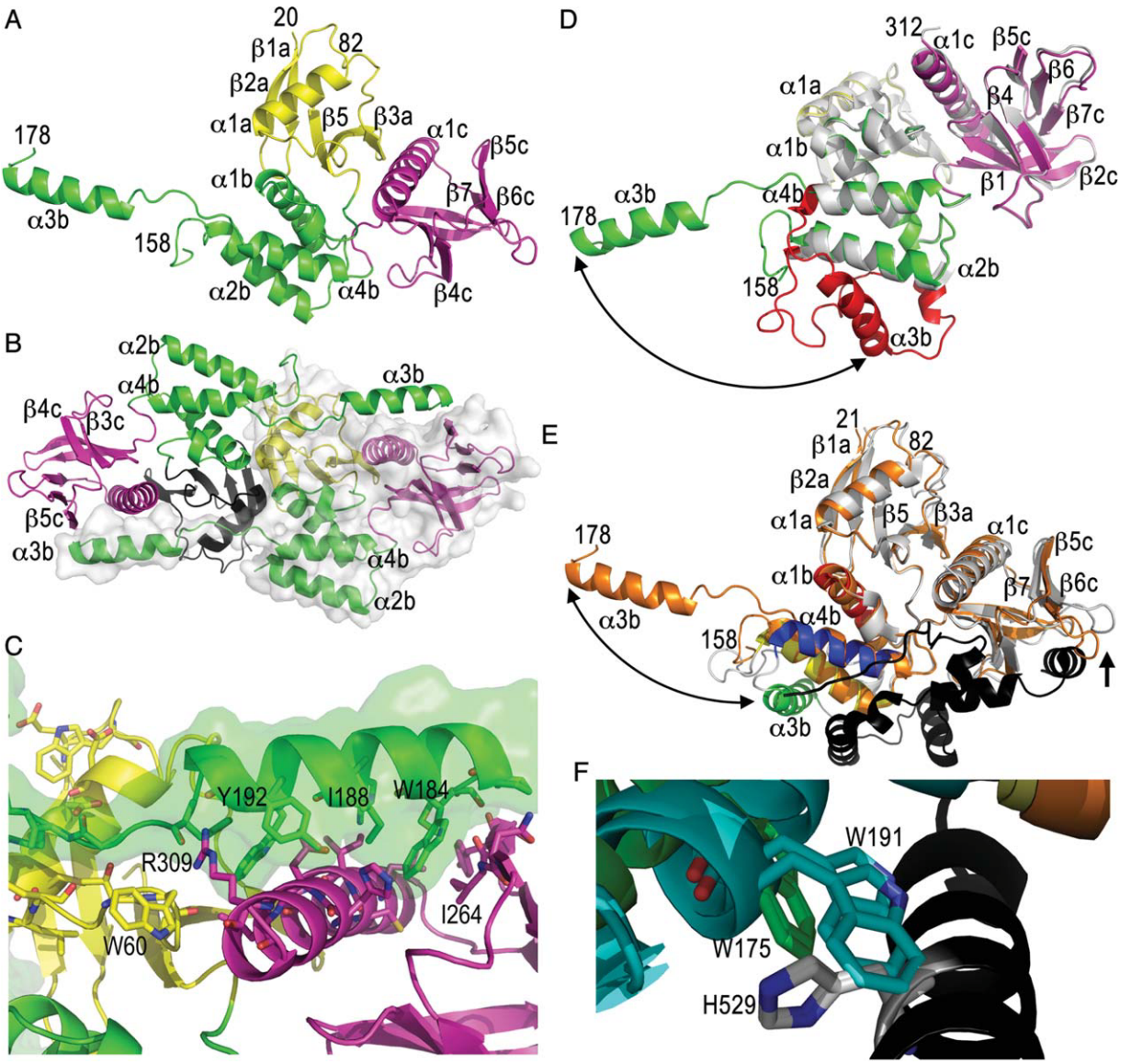

Figure 1. The merlin FERM domain structure is unfurled. (A) Cartoon drawing of the human merlin head FERM domain. The F1 subdomain (residues 20–82 and 91–100) is shown in yellow, the F2 subdomain (residues 101–158 and 178–215) is shown in green, and the F3 motif (residues 216–313) is shown in magenta. Some termini (21, 82, 158, and 178) and secondary structure elements ("a" belonging to the F1, "b" to F2, and "c" to the F3 subdomains) are labeled in several panels. (B) The unfurled F2 subdomain engages in additional contacts with another monomer, which is shown as a surface representation. The FERM subdomains are colored as in panel (A) (F1, yellow or black; F2, green; and F3, magenta). (C) Detailed view of the intermolecular interactions of the extended F2 α3b α-helix (F2, green) with a two-fold related molecule (F1, yellow; and F3, magenta). A surface representation is also shown for the F2 subdomain. (D) Superposition of our unfurled merlin head domain (molecule "C"; F1, yellow; F2, green; and F3, magenta) onto the closed, unbound FERM domain structure of merlin (PDB entry 1h4r; white and red) is shown. The two molecules in the closed FERM structure superimpose with r.m.s.d. of 1.3 and 1.4 Å for 1965 atoms of our unfurled merlin structure. The large movement of the α-helix α3b of the F2 subdomain (red) is indicated by the arrow. (E) Superposition of the unfurled merlin structure (molecule "C," orange) onto the moesin head:tail complex structure (PDB entry 1ef1; F1 and F2, white; F2 α-helix α1b, moesin residues 95–112, red; F2 α2b α-helix, moesin residues 118–135, yellow; F2 α3b α-helix, moesin residues 164–179, green; F2 α-helix α4b, moesin residues 183–196, blue; tail, black) with r.m.s.d. of 1.9 Å for 1780 atoms of the two moesin FERM domains in the asymmetric unit. The large movement of α-helix α3b is indicated by a double arrow. The movement of the β6c-β7c loop that seems necessary to allow tail binding is indicated by an arrow. (F) Close-up view of the movement of the α-helix α3b upon tail binding. Trp191 residing on the F2 α-helix α3b of the superimposed closed, unbound merlin FERM conformation clashes with the tail domain, in particular with His529.

similarities with the acyl-CoA binding protein, and F3 has structural homology to phosphotyrosine binding (PTB), pleckstrin homology (PH), and Enabled/VASP Homology 1 (EVH1) signaling domains. In particular, in all reported structures, the F2 FERM subdomain is comprised of four α-helices that form a compact bowl-like structure. To our surprise, the F2 subdomain of the merlin FERM domain is unfurled and the F2 α3b α-helix is rotated away from the remainder of this subdomain. The unfurled F2 subdomain is seen in all four subunits in the symmetric unit and all four subunits are very similar. The F2 α3b α-helix (residues 151–201) does not interact with the remainder of this subdomain as seen in the native structure of the merlin head domain alone[17] but with the α-helix α1c of the F3 subdomain of a two-fold related molecule [Fig. 1(B); Supporting Information Fig. S1]. Further, the loop that follows the F2 α-helix α2b (residues 151–158) engages in hydrophobic interactions with the side chains of Lys44, Asp45, Asp48, and Arg52 of the α-helix α1a of the F1 subdomain, and there are also electrostatic interactions between Asp152 and Arg52. In addition, the extended F2 α-helix α3b and its preceding region (residues 178–192) engage in hydrophobic contacts with Asn263, Ile264, Ser265, Leu297, Cys300, Ile301, Gly302, Asp305, and Leu306, which are located on the β-strand β5c (262–267) and α-helix α1c (290–311) of the two-fold related F3 subdomain [Fig. 1(C)]. Hydrogen-bond interactions of Met179 with Tyr266, Ile188 with Asp305, and Tyr192 with Arg309 are also manifest. Finally, the new extended loop connecting F2 α-helices α3b and α4b (residues 194–202) engages in hydrophobic interactions not seen in other FERM structures with the side chains of Cys51, Arg52, Arg57, Thr59, and Trp60, which are located on the two-fold related F1 subdomain α-helix α1a and its following loop. Hydrogen bond interactions of His195 with Arg309 and Arg198 with Leu56, Arg57, and Thr59 are also found in this contact area.

Superposition of our unfurled merlin head domain structure onto the 1.8 Å structure of the merlin head domain alone[17] shows that the F1 and F3 subdomains, and the α-helices α1b, α2b, and α4b regions of F2, are almost identical with r.m.s.d. of less than 0.6 Å for 1,704 atoms of residues 20–147 and 202–312 [Fig. 1(D)]. Similar results are obtained in a superposition with the mouse merlin FERM domain crystal structure.[18] However, in our structure the last turn of the α2b α-helix of the F2 subdomain unfurls, thereby extending the following loop region and moving α-helix α3b to a completely new position, which also results in movement of the *N*-terminus of the F2 α-helix α4b.

Superposition with the 3 Å full-length moesin crystal structure[33] (Supporting Information Fig. S2A) shows that the *C*-terminal region of the additional α-helix A of the central domain in moesin and the A–B loop prevents unfurling of its FERM domain. However, the central α-helical region, harboring α-helices A and B, is divergent between merlin and moesin with only 30% sequence identity.

Superposition with the moesin head:tail complex crystal structure [Fig. 1(E)] shows additional novel features of the F3 β6c-β7c loop (merlin residues 275–283), where this loop in our unfurled merlin FERM domain is located further away from the tail domain-binding site present in moesin, presumably to allow binding of the merlin-1 tail. Further, superposition of the closed, merlin structure, the moesin head–tail structure, and our unfurled head domain established that the β6c-β7c loop displays the conformation seen in the moesin head:tail complex structure allowing tail binding (Supporting Information Fig. S2B). Importantly, the F2 α-helix α3b, in particular Trp191 residing on α3b, prevents tail domain binding in the unbound merlin structure [Fig. 1(F)]. Indeed, the F2 α-helix α3b is shifted in the moesin head:tail structure to allow binding of the tail domain. Moreover, crystal contacts are not compatible with the tail binding as seen for moesin. We conclude that binding of the tail domain induces movements in the FERM domain, which could be initiating events for further unfurling of this region in merlin. Interestingly, there is only 43% identity in regions of divergent conformation (merlin residues 150–201), yet there is 53 and 74% identity in the 51 residues before (merlin residues 98–149) or after (merlin residues 202–253) this unfurled region (Supporting Information Fig. S3).

Dimerization

Full-length merlin-1 is a monomer in high salt (500 m*M*) yet forms homodimers and higher-order oligomers under physiological conditions.[29] Further, two-hybrid interaction analyses[34] and *in vitro* binding assays[35] suggest that the merlin-1 homodimer is the active form of the protein.[36] In our unfurled merlin head structure the interface between molecules A and C (or B and D) in the asymmetric unit is highly significant, where over 5,500 Å^2 total solvent accessible surface area is buried, corresponding to almost 18% of the solvent accessible surface area. Moreover, the shape correlation statistic derived using the CCP4 program SC[37] is 0.726 for this interface, a significant value where a value of 1 indicates perfect fit versus 0.35 indicates the mismatch of an artificial association. Further, the shape correlation statistics for the α-helix α3b of the F2 subdomain correspond to 0.801. These values suggest that the crystallographic dyad represents a homodimer in solution. Unfortunately, the heterogeneity of the protein domains prevented dynamic and static light scattering (DLS and SLS) experiments to determine their oligomeric state in solution (SDY, unpublished data),

a difficulty that has also been encountered by others.[29]

Discussion

We crystallized the merlin head:tail complex but electron density is only observed for the head domain; thus, the tail domain of merlin-1 is probably highly dynamic. Importantly, the binding of the tail domain provokes surprising movements and unfurling in the F2 motif of the merlin FERM domain. Further, this unfurling in the merlin head domain directs extensive interactions with a two-fold related molecule. To our knowledge the unfurling of any motif of the FERM domain is unprecedented and indeed all FERM structures are very similar. Thus, merlin stands alone in its architecture of this domain, which we propose plays important roles in merlin tumor suppressor functions. In support of this notion, the F2 subdomain was recently shown to be essential for merlin to suppress the proliferation of primary *Nf2*-deficient Schwann cells.[38] The merlin F2 domain also harbors a submotif called the blue box (177-YQMTPEM-183), which is conserved in other species but not in ERM proteins.[39] In *Drosophila*, a blue box mutant acts as a dominant negative, underscoring the importance of this region in merlin functions. Precisely how this motif contributes to merlin function is, however, unclear, as the blue box is disordered in our structure.

The extensive dyad interactions that are manifest in our unfurled merlin head domain structure are also unique for FERM domains. Although a dimeric 2.8 Å radixin structure[40] showed that a domain swap of the *C*-terminal β-strand is involved in dimeric interactions, those present in the merlin structure are six-fold greater in their buried accessible surface area. Indeed, this interface in the merlin structure (2,800 Å^2 per polypeptide chain) lies well within those observed for established homodimers, which range from 370 to 4,750 Å.[2,41] While large crystal contacts have been observed for up to 900 Å^2, at least for monomeric lysozyme,[42] the merlin FERM-FERM interface is more than three times greater than that of the unusually large crystal–crystal contacts of lysozyme.

Effects of salt on the oligomerization of full-length merlin-1 have been reported,[29] where increases in salt concentration have been suggested to sever the head:tail interaction and impair the higher-order oligomers present under physiological conditions. Indeed, the previously determined unbound merlin head domain structure was monomeric and crystallized in 56% saturated ammonium sulfate.[17] By contrast, our dimeric merlin head:tail complex crystallization was performed with 20-fold less ammonium sulfate. We hypothesize that tail domain-induced unfurling of the F2 subdomain directs dimerization and that this response is manifest in full-length merlin-1.

The structure presented herein provides important clues as to how merlin functions as a tumor suppressor. The head:tail structures of ERM proteins and of full-length moesin[33] have revealed a tight globular closed architecture. By contrast, our unfurled merlin FERM structure shows that at least the F2 subdomain is in an "open" configuration, where it may direct merlin-1 dimerization and/or its interactions with partners required for tumor suppression. Thus, loss-of-function mutations found in the head and tail domains in *Nf2* may prevent the binding of these open domains to other partners and/or dimerization of merlin-1, which may also be required for its tumor suppressor functions.

Materials and Methods

Protein preparation

Human *merlin-1* complementary DNA corresponding to its head domain (residues 18–312) was amplified and cloned into pGEX-6P-1 expression vector (GE Life Sciences) using the *Bam*HI and *Xho*I restriction sites. The untagged merlin-1 tail domain (residues 503–595) was amplified and cloned into pET24b expression vector (Novagen) using the *Nde*I and *Xho*I restriction sites. Proteins were expressed in *Escherichia coli* BL21(DE3)RIL (Stratagene) at 25°C for 20 h in Luria–Bertani medium with ampicillin (GST-head) or kanamycin (tail). Cells were pooled and lysed in 50 m*M* Tris, 300 m*M* NaCl (pH 8), and complete mini protease inhibitor tablet (Roche) and ultracentrifuged at 95,834*g* for 1 h. Proteins were copurified using a GST FF chromatography affinity column (GE Life Sciences) and eluted with 10 m*M* reduced glutathione. The GST-tag was removed by incubating 1 U PreScission protease per mg of protein in 50 m*M* Tris 150 m*M* NaCl, 1 m*M* DTT, 1 m*M* EDTA, pH 7.5, for 24 h at 4°C. The head:tail complex was further purified using a Superdex 75 26/60 gel filtration chromatography column (GE Life Sciences) equilibrated with 50 m*M* Tris and 300 m*M* NaCl (pH 8). The purified complex was concentrated to 5.6 mg mL^{-1}.

Crystallization and X-ray data collection and reduction

Initial crystallization hits were identified using the Lite crystallization screen (Hampton Research) at 4°C. Two similar conditions, both containing 200 m*M* ammonium sulfate and polyethylene glycol (PEG), produced microcrystals. Best crystals were obtained from 4.5% PEG-4000 and 0.2 *M* ammonium sulfate.

X-ray diffraction data were collected at the Advanced Photon Source, SER-CAT beamline 22ID,

Table I. *X-Ray Data Reduction and Crystallographic Refinement Statistics*

(A) X-ray data reduction statistics	
Space group	$P422$
Unit cell parameters ($a = b$, c)	105.45 Å, 330 Å
Wavelength	0.99999 Å
Resolution (last shell)	26.36–2.64 Å (2.78–2.64 Å)
R-merge[a] (last shell)	0.063 (0.377)
Total no. of observations	376,916 (12,653)
Total no. of unique reflections	52,570 (6182)
Average $I/\sigma(I)$ (last shell)	19.9 (1.9)
Completeness (last shell)	0.952 (0.797)
Redundancy (last shell)	7.2 (2)

(B) Crystallographic refinement statistics	
Space group	$P4_12_12$
Unit cell parameters ($a = b$, c)	105.45 Å, 330 Å
Low (high) resolution limit	38.65–2.64 Å (2.71–2.64 Å)
No. of reflections, working set (last shell)	49,850 (2626)
No. of reflections, test set (last shell)	2666 (128)
R-factor[b] (last shell)	0.2003 (0.2340)
R-free[c] (last shell)	0.2294 (0.2703)
No. of residues	1023
No. of protein atoms	8540
No. of solvent atoms	537
Average B-factor (protein)	65.8 Å^2
Average B-factor (solvent)	54.8 Å^2
Overall anisotropy B11, B22, B33	0.61620 Å^2, 0.61620 Å^2, 1.23240 Å^2
R.m.s.d. from ideal values	
Bond length	0.008 Å
Bond angle	0.87°

[a] $R\text{-merge} = \sum_{hkl}\sum_{i}|I_i(hkl) - \overline{I(hkl)}|/.\sum_{hkl}\sum_{i}I_i(hkl)$.

[b] $R\text{-factor} = \sum_{hkl}||F_{obs}(hkl)|-|F_{calc}(hkl)||/.\sum_{hkl}|F_{obs}(hkl)|$, where $<|F_{calc}|>$ denotes the expectation of $|F_{calc}(hkl)|$ used in defining the likelihood refinement target.

[c] The free R-factor is a cross-validation residual calculated by using about 5% reflections, which were randomly chosen and excluded from the refinement.

at the Argonne National Laboratory and processed with autoProc[43] utilizing XDS[44] and SCALA.[45] The data were reduced in space group P422, as the pattern of systematic absences precluded unambiguous assignment of the space group at this stage (Table I).

Structure determination and crystallographic refinement

Phases were obtained by molecular replacement using the merlin-1 head domain structure as a search model and the program PHASER.[46] We searched in all appropriate space groups and obtained four solutions in $P4_12_12$ and confirmed the space group with the CCP4 program SFTOOLS.[47] Eight rounds of crystallographic refinement were performed with autoBUSTER[48] with manual inspection and model building with Coot.[49] The first round of refinement included a cycle of rigid body refinement. Automatic LSSR NCS restraints[50] were applied throughout and water was added in the sixth round of refinement using the "findwater" routine in Coot.[49] The final crystallographic refinement statistics are shown in Table I.

PDB Coordinates

The coordinates have been deposited with the Protein Data Bank (PDB entry 3u8z).

Acknowledgment

The authors are indebted to colleagues at Scripps FL: Philippe Bois for initiating the project and fruitful discussions, John Cleveland for discussions and critical review of the manuscript, Zhen Wu and Philippe Bois for sequencing, and HaJeung Park and Erumbi Rangarajan for substantial help with data collection. They thank Kristie Rose for mass spectrometry experiments and peptide analyses. Finally, they are grateful to the staff at the Advanced Photon Source, SER-CAT, for their synchrotron support. SDY is a fellow of the Department of Defense Neurofibromatosis Research Program. This is publication number 20731 from The Scripps Research Institute.

References

1. McClatchey AI, Giovannini M (2005) Membrane organization and tumorigenesis—the NF2 tumor suppressor, Merlin. Genes Dev 19:2265–2277.
2. Stemmer-Rachamimov AO, Xu L, Gonzalez-Agosti C, Burwick JA, Pinney D, Beauchamp R, Jacoby LB, Gusella JF, Ramesh V, Louis DN (1997) Universal absence of merlin, but not other ERM family members, in schwannomas. Am J Pathol 151:1649–1654.
3. Ruttledge MH, Sarrazin J, Rangaratnam S, Phelan CM, Twist E, Merel P, Delattre O, Thomas G, Nordenskjold M, Collins VP, Dumanski JP, Rouleau GA (1994) Evidence for the complete inactivation of the NF2 gene in the majority of sporadic meningiomas. Nat Genet 6:180–184.
4. Bianchi AB, Mitsunaga SI, Cheng JQ, Klein WM, Jhanwar SC, Seizinger B, Kley N, Klein-Szanto AJ, Testa JR (1995) High frequency of inactivating mutations in the neurofibromatosis type 2 gene (NF2) in primary malignant mesotheliomas. Proc Natl Acad Sci USA 92:10854–10858.
5. Giovannini M, Robanus-Maandag E, van der Valk M, Niwa-Kawakita M, Abramowski V, Goutebroze L, Woodruff JM, Berns A, Thomas G (2000) Conditional biallelic Nf2 mutation in the mouse promotes manifestations of human neurofibromatosis type 2. Genes Dev 14:1617–1630.
6. McClatchey AI, Saotome I, Mercer K, Crowley D, Gusella JF, Bronson RT, Jacks T (1998) Mice heterozygous for a mutation at the Nf2 tumor suppressor locus develop a range of highly metastatic tumors. Genes Dev 12:1121–1133.
7. Lallemand D, Curto M, Saotome I, Giovannini M, McClatchey AI (2003) NF2 deficiency promotes tumorigenesis and metastasis by destabilizing adherens junctions. Genes Dev 17:1090–1100.

8. Curto M, Cole BK, Lallemand D, Liu CH, McClatchey AI (2007) Contact-dependent inhibition of EGFR signaling by Nf2/Merlin. J Cell Biol 177:893–903.
9. Maitra S, Kulikauskas RM, Gavilan H, Fehon RG (2006) The tumor suppressors Merlin and expanded function cooperatively to modulate receptor endocytosis and signaling. Curr Biol 16:702–709.
10. Brault E, Gautreau A, Lamarine M, Callebaut I, Thomas G, Goutebroze L (2001) Normal membrane localization and actin association of the NF2 tumor suppressor protein are dependent on folding of its N-terminal domain. J Cell Sci 114:1901–1912.
11. James MF, Manchanda N, Gonzalez-Agosti C, Hartwig JH, Ramesh V (2001) The neurofibromatosis 2 protein product merlin selectively binds F-actin but not G-actin, and stabilizes the filaments through a lateral association. Biochem J 356:377–386.
12. Xu HM, Gutmann DH (1998) Merlin differentially associates with the microtubule and actin cytoskeleton. J Neurosci Res 51:403–415.
13. Bretscher A, Edwards K, Fehon RG (2002) ERM proteins and merlin: integrators at the cell cortex. Nat Rev Mol Cell Biol 3:586–599.
14. Curto M, McClatchey AI (2008) Nf2/Merlin: a coordinator of receptor signalling and intercellular contact. Br J Cancer 98:256–262.
15. Pearson MA, Reczek D, Bretscher A, Karplus PA (2000) Structure of the ERM protein moesin reveals the FERM domain fold masked by an extended actin binding tail domain. Cell 101:259–270.
16. Smith WJ, Nassar N, Bretscher A, Cerione RA, Karplus PA (2003) Structure of the active N-terminal domain of Ezrin. Conformational and mobility changes identify keystone interactions. J Biol Chem 278:4949–4956.
17. Kang BS, Cooper DR, Devedjiev Y, Derewenda U, Derewenda ZS (2002) The structure of the FERM domain of merlin, the neurofibromatosis type 2 gene product. Acta Crystallogr D Biol Crystallogr 58:381–391.
18. Shimizu T, Seto A, Maita N, Hamada K, Tsukita S, Hakoshima T (2002) Structural basis for neurofibromatosis type 2. Crystal structure of the merlin FERM domain. J Biol Chem 277:10332–10336.
19. Edwards SD, Keep NH (2001) The 2.7 A crystal structure of the activated FERM domain of moesin: an analysis of structural changes on activation. Biochemistry 40:7061–7068.
20. Matsui T, Maeda M, Doi Y, Yonemura S, Amano M, Kaibuchi K, Tsukita S (1998) Rho-kinase phosphorylates COOH-terminal threonines of ezrin/radixin/moesin (ERM) proteins and regulates their head-to-tail association. J Cell Biol 140:647–657.
21. Shaw RJ, Paez JG, Curto M, Yaktine A, Pruitt WM, Saotome I, O'Bryan JP, Gupta V, Ratner N, Der CJ, Jacks T, McClatchey AI (2001) The Nf2 tumor suppressor, merlin, functions in Rac-dependent signaling. Dev Cell 1:63–72.
22. Hamada K, Shimizu T, Yonemura S, Tsukita S, Hakoshima T (2003) Structural basis of adhesion-molecule recognition by ERM proteins revealed by the crystal structure of the radixin-ICAM-2 complex. EMBO J 22:502–514.
23. Terawaki S, Maesaki R, Okada K, Hakoshima T (2003) Crystallographic characterization of the radixin FERM domain bound to the C-terminal region of the human Na+/H+-exchanger regulatory factor (NHERF). Acta Crystallogr D Biol Crystallogr 59:177–179.
24. Matsui T, Yonemura S, Tsukita S (1999) Activation of ERM proteins in vivo by Rho involves phosphatidylinositol 4-phosphate 5-kinase and not ROCK kinases. Curr Biol 9:1259–1262.
25. Fievet BT, Gautreau A, Roy C, Del Maestro L, Mangeat P, Louvard D, Arpin M (2004) Phosphoinositide binding and phosphorylation act sequentially in the activation mechanism of ezrin. J Cell Biol 164:653–659.
26. Laulajainen M, Muranen T, Carpen O, Gronholm M (2008) Protein kinase A-mediated phosphorylation of the NF2 tumor suppressor protein merlin at serine 10 affects the actin cytoskeleton. Oncogene 27:3233–3243.
27. Rong R, Surace EI, Haipek CA, Gutmann DH, Ye K (2004) Serine 518 phosphorylation modulates merlin intramolecular association and binding to critical effectors important for NF2 growth suppression. Oncogene 23:8447–8454.
28. Alfthan K, Heiska L, Gronholm M, Renkema GH, Carpen O (2004) Cyclic AMP-dependent protein kinase phosphorylates merlin at serine 518 independently of p21-activated kinase and promotes merlin-ezrin heterodimerization. J Biol Chem 279:18559–18566.
29. Nguyen R, Reczek D, Bretscher A (2001) Hierarchy of merlin and ezrin N- and C-terminal domain interactions in homo- and heterotypic associations and their relationship to binding of scaffolding proteins EBP50 and E3KARP. J Biol Chem 276:7621–7629.
30. Murthy A, Gonzalez-Agosti C, Cordero E, Pinney D, Candia C, Solomon F, Gusella J, Ramesh V (1998) NHE-RF, a regulatory cofactor for Na(+)-H+ exchange, is a common interactor for merlin and ERM (MERM) proteins. J Biol Chem 273:1273–1276.
31. Morrison H, Sherman LS, Legg J, Banine F, Isacke C, Haipek CA, Gutmann DH, Ponta H, Herrlich P (2001) The NF2 tumor suppressor gene product, merlin, mediates contact inhibition of growth through interactions with CD44. Genes Dev 15:968–980.
32. Hamada K, Shimizu T, Matsui T, Tsukita S, Hakoshima T (2000) Structural basis of the membrane-targeting and unmasking mechanisms of the radixin FERM domain. EMBO J 19:4449–4462.
33. Li Q, Nance MR, Kulikauskas R, Nyberg K, Fehon R, Karplus PA, Bretscher A, Tesmer JJ (2007) Self-masking in an intact ERM-merlin protein: an active role for the central alpha-helical domain. J Mol Biol 365: 1446–1459.
34. Scoles DR, Huynh DP, Morcos PA, Coulsell ER, Robinson NG, Tamanoi F, Pulst SM (1998) Neurofibromatosis 2 tumour suppressor schwannomin interacts with betaII-spectrin. Nat Genet 18:354–359.
35. Gutmann DH, Geist RT, Xu H, Kim JS, Saporito-Irwin S (1998) Defects in neurofibromatosis 2 protein function can arise at multiple levels. Hum Mol Genet 7: 335–345.
36. Stokowski RP, Cox DR (2000) Functional analysis of the neurofibromatosis type 2 protein by means of disease-causing point mutations. Am J Hum Genet 66: 873–891.
37. Lawrence MC, Colman PM (1993) Shape complementarity at protein/protein interfaces. J Mol Biol 234:946–950.
38. Lallemand D, Saint-Amaux AL, Giovannini M (2009) Tumor-suppression functions of merlin are independent of its role as an organizer of the actin cytoskeleton in Schwann cells. J Cell Sci 122:4141–4149.
39. LaJeunesse DR, McCartney BM, Fehon RG (1998) Structural analysis of Drosophila merlin reveals functional domains important for growth control and subcellular localization. J Cell Biol 141:1589–1599.
40. Kitano K, Yusa F, Hakoshima T (2006) Structure of dimerized radixin FERM domain suggests a novel masking motif in C-terminal residues 295–304. Acta

Crystallogr Sect F Struct Biol Cryst Commun 62: 340–345.
41. Henrick K, Thornton JM (1998) PQS: a protein quaternary structure file server. Trends Biochem Sci 23: 358–361.
42. Janin J, Rodier F (1995) Protein-protein interaction at crystal contacts. Proteins 23:580–587.
43. Vonrhein C, Flensburg C, Keller P, Sharff A, Smart O, Paciorek W, Womack T, Bricogne G (2011) Data processing and analysis with teh autoPROC toolbox. Acta Crystallogr D Biol Crystallogr 67:293–302.
44. Kabsch W (2010) XDS. Acta Crystallogr D Biol Crystallogr 66:125–132.
45. Evans P (2006) Scaling and assessment of data quality. Acta Crystallogr D Biol Crystallogr 62:72–82.
46. McCoy AJ, Grosse-Kunstleve RW, Adams PD, Winn MD, Storoni LC, Read RJ (2007) Phaser crystallographic software. J Appl Crystallogr 40:658–674.
47. Collaborative Computational Project N (1994) The CCP4 Suite: programs for protein crytsallography. Acta Crystallogr D Biol Crystallogr D50:760–763.
48. Bricogne G, Blanc E, Brandl M, Flensburg C, Keller P, Paciorek P, Roversi P, Sharff A, Smart O, Vonrhein C, Womack T (2010) BUSTER version 2.9. Cambridge, United Kingdom: Global Phasing Ltd.
49. Emsley P, Cowtan K (2004) Coot: model-building tools for molecular graphics. Acta Crystallogr D Biol Crystallogr 60:2126–2132.
50. Smart OS, Brandl M, Flensburg C, Keller P, Paciorek W, Vonrhein C, Womack TO, Bricogne G (2008) Refinement with local structure similarity restraints (LSSR) enables exploitation of information from related structures and facilitates use of NCS. Abstr Annu Meet Am Crystallogr Assoc, Knoxville, TN. abstr. TP139.